J. Electrochem. Sci. Eng. **16** (2026) 3207; https://doi.org/10.5599/jese.3207

Open Access : : ISSN 1847-9286
https://pub.iapchem.org/ojs/index.php/JESE

Original scientific paper

Phenolic-rich plum peel extract-mediated synthesis of gold nanoparticles for electrochemical detection of Pb(II)

Yohanes Susanto Ridwan[1,2], Muhammad Fajar Arzena Nurhadi[3], Santhy Wyantuti[1,4], Rafa Radithya Swara[4], Athanasia Amanda Septevani[2], Fitri Khoerunnisa[3], Irkham[1,4,✉] and Yeni Wahyuni Hartati[1,4,✉]

[1]*Department of Chemistry, Faculty of Mathematics and Natural Science, Universitas Padjadjaran, Jalan Raya Bandung-Sumedang Km 21 Jatinangor, Sumedang 45363, Indonesia*
[2]*Research Center for Electronics, Research Organization of Electronics and Informatics, National Research and Innovation Agency Republic of Indonesia, Jakarta 10340, Indonesia*
[3]*Departement of Chemistry, Faculty of Mathematics and Natural Science, Universitas Pendidikan Indonesia, Jl. Dr. Setiabudi No.229, Kota Bandung 40154, Indonesia*
[4]*Study Center of Sensor and Green Chemistry, Faculty of Mathematics and Natural Science, Universitas Padjadjaran, Bandung 40132, Indonesia*

Corresponding Authors: ✉ irkham@unpad.ac.id; ✉ yeni.w.hartati@unpad.ac.id

Received: January 5, 2026; Accepted: April 11, 2026; Published: March xx, 2026

Abstract

Gold nanoparticles (AuNPs) were successfully synthesized using plum peel (Prunus salicina) extract as a green reducing and stabilizing agent, offering an environmentally benign approach to nanomaterial preparation. Optimization showed that a precursor-to-extract volume ratio of 7:3 with 80 mL maceration solvent yielded the most stable colloid, evidenced by a surface plasmon resonance peak at 534.9 nm. Fourier transform infrared spectroscopy analysis indicated that phenolic -OH and aromatic C=O/C=C functional groups played a key role in Au(III) reduction and nanoparticle stabilization. Transmission electron microscopy images revealed predominantly spherical AuNPs with an average size of 13.16±4.9 nm, while a zeta potential of -33.4 ± 0.2 mV confirmed colloidal stability. The optimized AuNPs were drop-casted onto pencil graphite electrodes (PGE) to fabricate a low-cost electrochemical sensor for Pb(II) detection. The modified electrode exhibited a 50.7% enhancement in the Pb(II) peak current compared to bare PGE. Differential pulse voltammetry showed linearity over 25 to 200 ppb (R^2 = 0.9921), a sensitivity of 0.0172 μA ppb^{-1}, and a limit of detection of 18.95 ppb, below the Indonesian regulatory limit for surface waters. Scanning electron microscopy-energy dispersive X-ray spectroscopy mapping confirmed uniform AuNPs distribution, supporting improved electron-transfer behaviour. Overall, this work highlights the potential of fruit-peel-derived AuNPs for a portable and sustainable detector.

Keywords
Noble metal nanoparticles; green synthesis; plant extract; lead detection; pencil graphite; sustainable management

Introduction

Ionic lead, Pb(II), is a persistent heavy metal pollutant that poses serious risks to environmental quality and human health [1,2]. Once released into aquatic systems through industrial discharge, mining activities, battery waste, and urban runoff, Pb(II) can bioaccumulate in sediments and aquatic organisms, ultimately entering the food chain. Even at trace levels, Pb(II) exposure is associated with neurological, renal, and developmental disorders. According to Dicky *et al.* [3], who investigated the concentration of heavy metal Pb(II) in the bottom sediments of the Eastern Flood Canal waters in Semarang, Pb(II) pollution in marine environments generally originates from transportation activities. Their findings indicated that the concentration of Pb(II) in the bottom sediments ranged from 14.3 to 31.35 ppm, with an average value of 21.82 ppm. The highest concentration was observed in the offshore area, far from the river mouth. Lead is contained in fuels as an anti-knock agent and is released into the atmosphere through exhaust emissions, after which it dissolves in seawater. Once introduced into the ecosystem, lead can accumulate in marine organisms such as fish, shrimp, and shellfish, which may subsequently be consumed by humans, and can be potentially poisonous [3,4]. Therefore, rapid and reliable monitoring of Pb(II) contamination in water sources is crucial.

Standard analytical techniques, particularly atomic absorption spectrometry (AAS) and inductively coupled plasma mass spectrometry (ICP-MS), offer high accuracy but require expensive instrumentation, specialized operators, intensive sample preparation, and centralized laboratory facilities. These limitations hinder their applicability for on-site or routine monitoring, especially in resource-limited settings.

Electrochemical techniques have emerged as promising alternatives for decentralized detection of heavy metals owing to their high sensitivity, operational simplicity, low power consumption, and capability for miniaturization. Among electrochemical methods, differential pulse voltammetry (DPV) provides excellent analytical performance due to its ability to suppress capacitive background currents, thereby improving signal resolution. The effectiveness of an electrochemical sensor, however, is strongly dependent on the properties of its working electrode. Pencil graphite electrodes (PGEs) are particularly attractive because they are inexpensive, disposable, widely available, and easy to modify [5,6]. Nonetheless, unmodified PGEs often suffer from limited sensitivity and insufficient active surface area, which limits their applicability for trace metal detection. This challenge can be addressed by modifying the electrode with nanomaterials.

Gold nanoparticles (AuNPs) are among the most widely used nanomaterials for enhancing electrochemical sensor performance [7]. Their large surface-to-volume ratio, high electrical conductivity, and catalytic activity significantly improve electron-transfer kinetics and increase the density of active sites on the electrode surface. AuNPs also facilitate adsorption and underpotential deposition (UPD) of metal ions such as Pb(II), resulting in stronger and more defined voltammetric responses [8,9]. Conventional AuNPs synthesis, however, typically involves chemical reductants such as sodium borohydride or citrate, which may generate hazardous waste and require strict handling. These drawbacks underscore the need for greener, more sustainable synthesis routes.

In recent years, green synthesis of metal nanoparticles using plant extracts has gained substantial attention due to its environmental friendliness, low cost, and biocompatibility. Plant-derived

phytochemicals, such as polyphenols, flavonoids, and organic acids, act as natural reducing and stabilizing agents, eliminating the need for harsh chemicals [10]. Importantly, the efficiency of plant-mediated nanoparticle formation is not only determined by the plant species used but is largely determined by the specific phytochemical composition of the extract. Phenolic compounds containing hydroxyl groups and conjugated aromatic systems can donate electrons to metal ions, facilitating their reduction, while oxygen-containing functional groups allow adsorption on the nanoparticle surface, thus providing electrostatic stabilization. Previous phytochemical analysis of *Prunus salicina* peel has identified hydroxycinnamic acids such as ferulic acid (47.87 mg kg^{-1}) and sinapic acid, as well as flavonoids including quercetin, gallic acid derivatives, and anthocyanins in significant concentrations [11]. These phenolic constituents possess numerous hydroxyl groups and conjugated π-electron systems capable of electron donation and metal ion chelation, thus providing a rational chemical basis for controlled Au(III) reduction and nanoparticle stabilization rather than representing a simple substitution of plant extracts. Phenolic-driven reduction and surface passivation are expected to affect the nanoparticle size distribution, surface charge, and interfacial electron transfer properties, thus directly impacting the electrochemical sensing performance. Despite this chemical richness, the use of plum peel extract for AuNPs synthesis and its application in electrochemical heavy-metal sensing remains very limited in the literature.

Furthermore, although PGE-modified AuNPs have been explored for various sensing applications, few studies have systematically evaluated whether phytochemical-mediated AuNPs, synthesized under optimized precursor-to-extraction conditions, can regulate the nucleation growth behaviour of nanoparticles and translate these structural characteristics into improved electrochemical detection performance. Establishing a structure-property-performance relationship is crucial for advancing the design of sustainable nanomaterial-based sensors.

This study addresses the aforementioned gaps by developing a green synthesis approach for AuNPs using plum peel extract and applying the resulting nanoparticles to modify PGEs for Pb(II) sensing. The work consists of three major components: (i) optimization of AuNPs synthesis parameters by varying the precursor-to-extract ratio and extraction solvent volume; (ii) physicochemical characterization of the synthesized AuNPs using UV-Vis spectrophotometry, Fourier transform infrared (FTIR) spectroscopy, transmission electron microscopy (TEM), scanning electron microscopy (SEM) and zeta potential measurements; and (iii) evaluation of the analytical performance of AuNPs-modified PGEs for Pb(II) detection using DPV. The optimized AuNPs were deposited onto the PGE surface *via* a straightforward drop-casting method to create a conductive, nanoparticle-enriched interface. Sensor performance was assessed in terms of peak current enhancement, linearity, sensitivity, detection limit, and quantification limit.

By integrating the valorisation of agricultural waste with mechanistically rational nanoparticle formation, this study demonstrates that phenolic-rich plum peel extract mediates AuNPs synthesis and surface stabilization, ultimately enhancing voltammetric detection of Pb(II).

Experimental

Materials

Gold(III) chloride trihydrate ($HAuCl_4 \cdot 3H_2O$), ethanol (70 %), methanol (analytical grade), distilled water, polyvinylpyrrolidone (PVP), PTFE tubing, and Whatman No. 1 filter paper were used as received. Pencil graphite rods (2 mm diameter) were obtained from commercial mechanical pencil leads. Fresh Chinese plum peel (*Prunus salicina*) was used as the source of plant extract for green synthesis. All reagents were of analytical grade.

Instrumentation

UV-Vis spectra were recorded using an Agilent spectrophotometer (Agilent Technologies, USA). FTIR analysis was conducted using a Thermo Scientific Nicolet iS5 spectrometer (Thermo Fisher Scientific, USA). Particle morphology and size distribution were examined using a Talos F200X transmission electron microscope (Thermo Fisher Scientific, USA). Surface morphology and elemental composition of electrodes were analysed using a JEOL JSM-6510 scanning electron microscope equipped with energy dispersive X-ray spectroscopy (JEOL Ltd., Japan). Zeta potential measurements were performed using a HORIBA SZ-100 (HORIBA Ltd., Japan). Electrochemical experiments (CV and DPV) used a Metrohm Autolab PGSTAT101 potentiostat controlled by NOVA software (Metrohm Autolab B.V., Netherlands).

Preparation of plum peel extract

Fresh plum peels (20 g) were washed, weighed, and macerated in 60, 70 or 80 mL of distilled water for 24 h at room temperature in a covered container. The mixture was filtered through Whatman No. 1 paper, and the filtrate was collected as the extract stock solution for nanoparticle synthesis.

Green synthesis and optimization of gold nanoparticles

A total of nine synthesis conditions were prepared by combining three extract volumes (3, 4 and 5 mL) with three maceration solvent volumes (60, 70 and 80 mL), while keeping the $HAuCl_4$ precursor constant at 7 mL of 0.001 M solution. The extract was added dropwise to the precursor under continuous stirring for 30 min. Formation of AuNPs was monitored visually (colour change) and confirmed by UV-Vis spectroscopy. The condition showing the most intense and stable plasmonic peak was selected as the optimized AuNPs formulation. The synthesized dispersions were centrifuged at 10,000 rpm for 10 min, and the pellets were washed twice with distilled water. Approximately 300 mg of the purified pellet was collected for electrode modification.

Preparation and activation of the pencil graphite electrode

Pencil graphite rods (~6 cm length) were ultrasonically cleaned in 70 % ethanol (5 min) followed by distilled water (5 min) and air-dried. The electrode surface was polished on plain paper using a figure-eight motion to achieve a smooth, uniform surface. The graphite rod was inserted into a PTFE sleeve, connected to a copper wire for electrical contact, and sealed with parafilm, leaving only the tip exposed. Electrochemical activation was performed in 0.5 M H_2SO_4 by cyclic voltammetry (three cycles, +0.5 to +1.5 V *vs.* Ag/AgCl, 0.1 V s^{-1}) to remove surface impurities and enhance electrode activity.

Modification of pencil graphite electrode with gold nanoparticles

The AuNPs pellet obtained from the optimized synthesis was redispersed in 1 mL of a 1:1 (v/v) water-ethanol mixture containing 0.025 g PVP. A volume of 5 µL of the AuNPs dispersion was drop-cast onto the activated PGE tip and dried for 8 h at room temperature. This deposition process was repeated four times to obtain a uniform AuNPs layer. Modified electrodes were stored in a dust-free container prior to electrochemical analysis.

Electrochemical measurements

A three-electrode system was used, consisting of the PGE or AuNPs-modified PGE as the working electrode, Ag/AgCl (3 M KCl) as the reference electrode and platinum wire as the counter electrode. DPV measurements for Pb(II) detection were carried out in 0.1 M KCl supporting electrolyte. The DPV

parameters were: start potential: -0.8 V, end potential: -0.2 V, step potential: 0.005 V, modulation amplitude: 0.025 V, modulation time: 0.05 s, interval time: 0.5 s.

Peak currents were obtained for Pb(II) standard solutions of 50 ppm (for electrode screening) and 25 to 200 ppb (for calibration). Sensor performance was evaluated using linear regression, sensitivity (slope), limit of detection (LOD), and limit of quantification (LOQ). The standard deviation for LOD/LOQ calculations was determined from repeated measurements (n = 3) of the lowest detectable Pb(II) concentration when blank signals were not measurable.

Characterization of extract, gold nanoparticles and modified electrodes

The plum extract and synthesized AuNPs were characterized by UV-Vis and FTIR to verify nanoparticle formation and identify functional groups involved in reduction/capping. TEM was used to determine particle morphology and size distribution. Zeta potential measurements evaluated colloidal stability. Scanning electron microscopy-energy dispersive X-ray spectroscopy (SEM-EDX) analysis assessed the surface morphology, AuNPs distribution, and elemental composition of bare and modified PGEs.

Results and discussion

Plum skin extraction

The plum peels used in this study were taken from a local home industry in Bandung, Indonesia. In this study, the peels were first washed thoroughly with running water, weighed (20 g), and then extracted by maceration. The extraction was carried out by soaking the samples in 60 mL, 70 mL, and 80 mL of distilled water for 24 hours under plastic wrap, followed by filtration through Whatman No. 1 filter paper. In principle, maceration facilitates the transfer of soluble components from a solid matrix into a solvent through diffusion, driven by the concentration gradient (Fick's Law) and the polarity compatibility between the solvent and solute [12]. Since the primary target compounds in this study were hydrophilic substances with potential roles as bioreducing and/or stabilizing (capping) agents, such as polyphenols, polysaccharides, and organic acids, water was selected as the solvent due to its polarity. This promotes the dissolution of functional groups such as -OH (phenolic/alcohol) and C-O/C-O-C (alcohol/ether/glycosidic). Additionally, this solvent may also extract other groups and metabolites, including polysaccharides and secondary metabolites [13]. The extract also contains carbohydrate fractions derived from the cell walls of the plum peel.

It is important to keep the container tightly closed during maceration to minimize phenolic oxidation and to reduce the volatilization of volatile components. The resulting filtrate was stored in a refrigerator at approximately 4 °C. This filtrate was subsequently used as the stock extract solution for the AuNPs synthesis and characterization stages [14]. As shown in Figure 1, a noticeable colour change occurred during the maceration process.

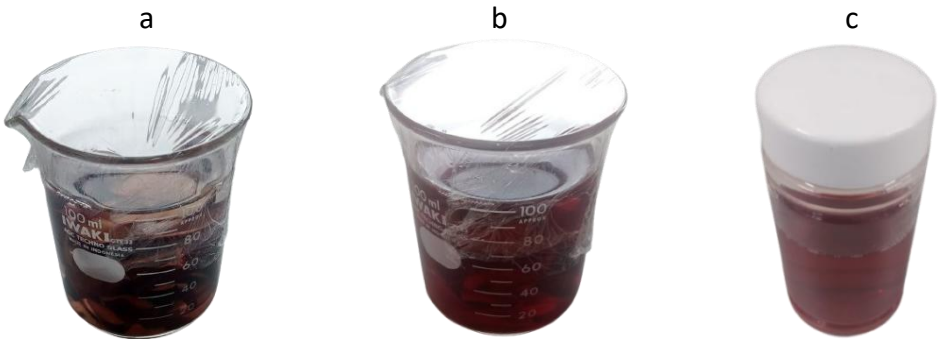

Figure 1. *(a) Maceration of plum skin, (b) maceration after 24 hours, and (c) plum skin extract*

Initially, the distilled water was clear and colourless after being left for 24 hours in a closed container, but it turned dark red. Following filtration, the colour of the extract became bright red, indicating the successful extraction of coloured bioactive compounds from the plum skin.

Synthesis of gold nanoparticles

The synthesis of AuNPs in this study was carried out using a green synthesis approach, employing plum fruit peel extract as a dual-function agent: a reducing agent for converting Au(III) to Au(0), and a stabilizing (capping) agent for particle surface stabilization [15]. The process was conducted in an aqueous medium derived from both the $HAuCl_4$ precursor solution and the plum peel extract. The purpose of using a green synthesis approach was to minimize the use of hazardous reagents and high-energy processes while using natural compounds as both reducing agents and stabilizers, enabling the reaction to proceed in water at room temperature.

An aqueous $HAuCl_4$ precursor solution (1 mM) was added (7 mL) to a 20 mL beaker. The precursor volume was kept constant during the optimization process to maintain consistent conditions, including Au(III) concentration, acidity and chloride speciation, and to ensure that variations in reaction outcomes could be attributed primarily to differences in the amount of extract added.

The plum peel extract was added dropwise into the $HAuCl_4$ solution while stirring continuously for 30 minutes. Gradual addition with constant stirring aimed to prevent local concentration gradients of reducing/capping agents, promoting a more uniform reaction and homogeneous nucleation throughout the solution. The extract volume (3 to 5 mL) was used as a variable to adjust the precursor-to-reducing/capping ratio without altering the total amount of gold. The 30-minute stirring time was selected as an optimal compromise to ensure sufficient reagent contact and diffusion without additional heating, in line with green chemistry principles. During this process, a visible colour change occurred with increasing reaction time, as shown in Figure 2.

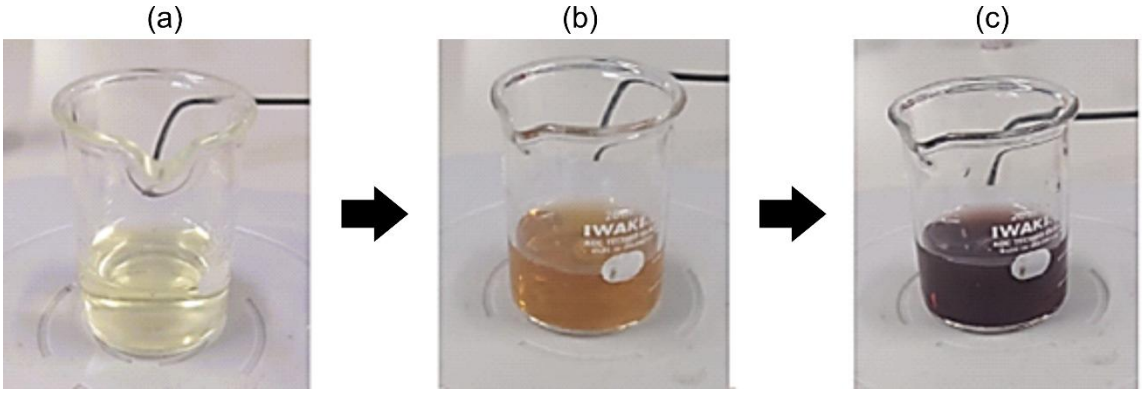

Figure 2. *AuNPs synthesis process: (a) $HAuCl_4$ precursor solution, (b) mixing plum skin extract, (c) synthesized AuNPs after stirring for 30 minutes*

Optimization of gold nanoparticle synthesis

In this study, the following two variables were investigated: (1) the solvent volume used during maceration extraction, set at 60, 70 and 80 mL, and (2) the volume ratio between the $HAuCl_4$ precursor solution and the plum peel extract, varied at 7:3, 7:4 and 7:5. The volume of the $HAuCl_4$ precursor was kept constant due to its relatively high cost and to minimize pH shifts that could alter the reaction kinetics and reduction mechanism of Au(III). Since $HAuCl_4$ is acidic, changing its volume would affect the acidity of the medium, which in turn influences the protonation degree of reducing functional groups as well as the nucleation and growth rates of gold nanoparticles. By maintaining a more controlled, comparable pH across conditions, the influence of these factors can be

minimized. Furthermore, keeping the precursor volume constant also helps control the chloride speciation effect that can impact particle size or aggregation. $HAuCl_4$ contributes Cl^- ions to the system; the concentration of Cl^- can affect surface charge, early-stage aggregation, and even etching processes on gold surfaces. Consequently, maintaining a constant precursor volume ensures a consistent Cl^- background, preventing variations in nanoparticle size or absorbance that could arise from changes in chloride concentration or ionic speciation.

Based on the two predetermined variables, an experimental design was established as shown in Table 1.

Table 1. *Experimental design for the optimization of AuNPs synthesis*

Sample	F1	F2	F3	F4	F5	F6	F7	F8	F9
Volume ratio of precursor to peel extract	7:3	7:3	7:3	7:4	7:4	7:4	7:5	7:5	7:5
Volume of aquadest, mL	60	70	80	60	70	80	60	70	80

The synthesis procedure was carried out as previously described by mixing a specific volume of plum peel extract (obtained by maceration using different solvent volumes) with a fixed volume of the $HAuCl_4$ precursor solution (7 mL). The resulting colloidal AuNPs are shown in Figure 3.

Figure 3. *Results of AuNPs optimization variation experiments according to Table 1*

Visually, the AuNPs sample coded as F3 exhibited the most intense reddish-purple colour among all experiments. Compared with other samples showing relatively high colour intensity, such as F1, F7, and F9. AuNPs F3 also displayed better colloidal stability, as no significant aggregation or precipitation of nanoparticles into larger particles was observed.

To accurately determine the optimal synthesis condition, all samples were characterized using UV-Vis spectrophotometry to identify the one with the highest absorbance. Optimization based on the maximum absorbance response has also been widely employed in previous studies. For instance, Tyagi *et al.* [16] optimized gold nanoparticle synthesis using sodium citrate *via* the Turkevich method, with pH and the precursor-to-reductant ratio as variables.

As shown in Figure 4, the results revealed that sample F3 exhibited the best optical response, with an absorbance (A) of $A_{max} = 0.403$ at $\lambda_{max} = 534.9$ nm. Therefore, F3 was selected as the optimum condition based on its absorbance profile.

Higher A_{max} value under identical optical settings indicates a greater effective particle concentration, while the stable peak position around ~535 nm suggests that the increase in absorbance was not accompanied by significant particle growth or aggregation, which typically results in a red-shift. Thus, F3 represents the most favourable balance between nucleation and growth among the tested formulations.

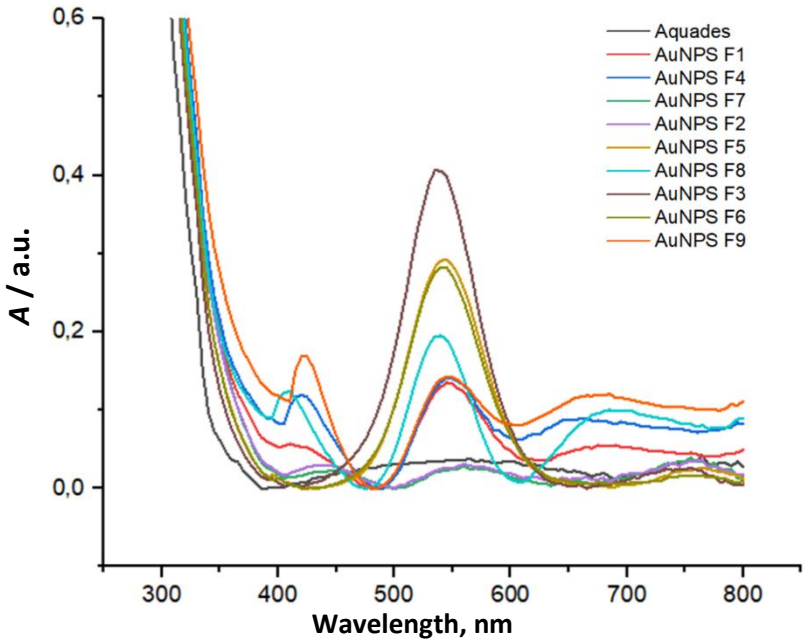

Figure 4. *UV-Vis spectra of nine AuNPs experimental samples F1-F9*

Higher A_{max} value under identical optical settings indicates a greater effective particle concentration, while the stable peak position around ~535 nm suggests that the increase in absorbance was not accompanied by significant particle growth or aggregation, which typically results in a red-shift. Thus, F3 represents the most favourable balance between nucleation and growth among the tested AuNPs formulations.

Preparation and modification of pencil graphite electrode

The graphite core was first cut to approximately 10 cm, immersed in 70% ethanol, and cleaned ultrasonically for 5 minutes, followed by rinsing with deionized water to remove residual solvent. This step standardizes the electrode geometry (making it easier to handle and providing a more consistent surface area) while removing binders and organic impurities, yielding a cleaner, more reproducible surface for electrochemical measurements [17]. The graphite tip was then polished on paper using a figure-eight motion. The figure-eight pattern was chosen because it continuously changes the polishing direction, resulting in multidirectional (more isotropic) surface scratches, a more uniform pressure distribution, and a reduced formation of long grooves that could alter the effective surface area. The figure-eight polishing technique is widely recommended in the preparation of carbon-based electrodes [18]. The graphite rod was then inserted into a PTFE tube, connected to a copper wire at the back end for electrical contact, and sealed with parafilm so that only the tip was exposed to the electrolyte solution. This design provides a well-defined geometric area, prevents electrolyte leakage into the electrode body, and ensures stable electrical contact. Such electrode configuration and insulation are commonly applied for PGE and glassy carbon electrodes in electrochemical sensor applications.

Prior to use, the electrode was electrochemically activated by cyclic voltammetry (CV) in 0.5 M H_2SO_4 for three cycles. Electrochemical activation in sulfuric acid is widely used because the CV cycles help remove residual binders or impurities from the graphite and generate oxygen-containing surface functional groups (-OH, >C=O, -COOH) [19]. As a result, the surface becomes more hydrophilic and better suited for electron transfer. This behaviour has been well-documented for carbon-based electrodes, particularly glassy carbon, and forms the basis of standard activation

practices for PGE. Activation with dilute H_2SO_4 is preferred for its simplicity, low cost, and reproducibility in carbon surface standardization.

The modification of PGE was carried out using AuNPs obtained as pellets from centrifugation, which were redispersed in 1 mL of a mixed solvent of deionized water and 70 % ethanol (1:1 v/v) containing 0.025 g of polyvinylpyrrolidone (PVP) as a mild surfactant and binder. The water-ethanol mixture was chosen to lower the surface tension, thereby improving wetting on the carbon surface and controlling the drying pattern by reducing the coffee-ring effect through Marangoni flow in the binary solvent. Meanwhile, PVP stabilized the AuNPs during deposition and promoted film adhesion to the graphite surface.

The AuNPs suspension (5 µL) was drop-cast onto the exposed tip of the PGE, air-dried for approximately 8 hours, and this process was repeated until four layers were formed. The small deposition volume (≈5 µL) ensured controlled film thickness and uniform coverage over the working area. Prolonged drying facilitated the formation of a more compact and homogeneous film, while sequential multilayer deposition improved surface coverage and minimized local defects, without requiring a larger single-drop volume.

As can be seen in Figure 5, modification of carbon electrodes with AuNPs *via* drop-casting provides a simple, reproducible, and widely adopted approach in electrochemical sensor fabrication (*e.g*. GCE, SPCE or PGE). This method effectively attaches AuNPs to the graphite surface without specialized equipment and is consistent with recent studies reporting AuNPs-modified carbon electrodes that exhibit enhanced interfacial electrochemical performance.

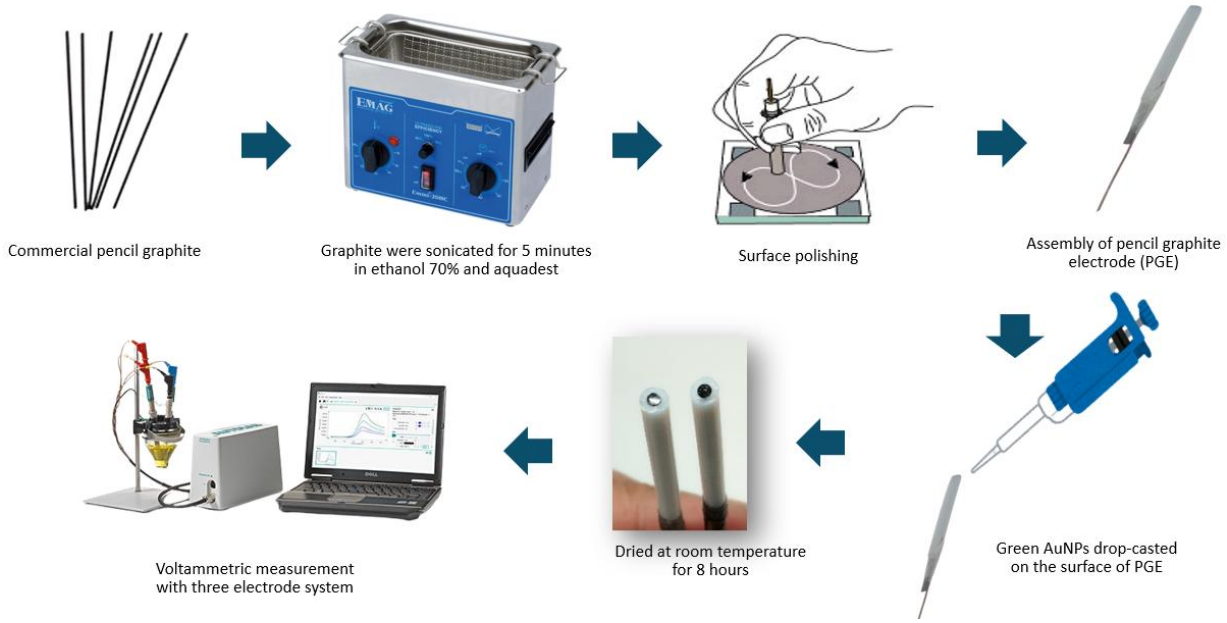

Figure 5. *Process of modification of pencil graphite electrode using green synthesized AuNPs*

Characterization of optimized gold nanoparticles

UV-Vis spectroscopy

UV-Vis spectrophotometry operates by passing light of various wavelengths through a sample and measuring the amount of light absorbed. AuNPs exhibit strong absorption at specific wavelengths due to the phenomenon known as localized surface plasmon resonance (LSPR). LSPR occurs when free electrons on the surface of metal nanoparticles collectively oscillate in response to incident light at a particular frequency [20]. This collective oscillation produces intense light absorption at the resonance wavelength, enabling gold nanoparticles to efficiently absorb visible

light (particularly in the green region) and thereby impart a characteristic red color to the colloidal solution. The absorbance peak observed at 534.9 nm is a direct manifestation of the LSPR of AuNPs, where the conduction electrons of gold resonate with visible light at that wavelength. As a result, the absorbance intensity near $\lambda \approx 534$ nm is significantly higher than that of non-plasmonic materials, even at relatively low nanoparticle concentrations [21].

Qualitative UV-Vis characterization was performed on the most optimal AuNPs sample, designated as F3, prepared using a precursor-to-extract ratio ($HAuCl_4$ solution: plum peel extract) of 7:3 volume ratio (Figure 6). The extract used in this synthesis was obtained by maceration with 80 mL of distilled water. The UV-Vis spectrum of the optimized AuNPs (sample F3) exhibited an absorbance value of 0.403 with an LSPR peak at 534.9 nm. The presence of a single, well-defined absorption peak around 534 nm is a characteristic feature of the LSPR behavior of gold nanoparticles. This result is consistent with previous literature, in which AuNPs synthesized using fruit extracts (including plum-derived extracts) typically exhibit plasmon resonance peaks within the 520-550 nm range [22]. The formation of a distinct peak at 534.9 nm thus confirms the successful reduction of Au(III) ions to metallic Au(0) nanoparticles, as evidenced by the appearance of a characteristic wine-red colour in the colloidal solution [23]. Similar A_{max} were found by Sathya *et al.* using papaya peel extracts [24].

The appearance of a single LSPR peak at 534.9 nm, without any additional peaks, indicates that the synthesized gold nanoparticles are relatively uniform in size and well-dispersed (spherical and not significantly aggregated). The λ_{max} at approximately 534.9 nm falls within the typical range for nanometre-sized AuNPs. For comparison, very small gold nanoparticles (~5 to 10 nm) generally exhibit SPR peaks around 520 nm, whereas larger particles (~50 nm) display a red-shift toward ~550 nm. Therefore, the λ_{max} at 534.9 nm suggests that the gold nanoparticles produced in this study are likely within the tens-of-nanometres size range, in good agreement with the average diameter (~13 nm) determined by TEM analysis.

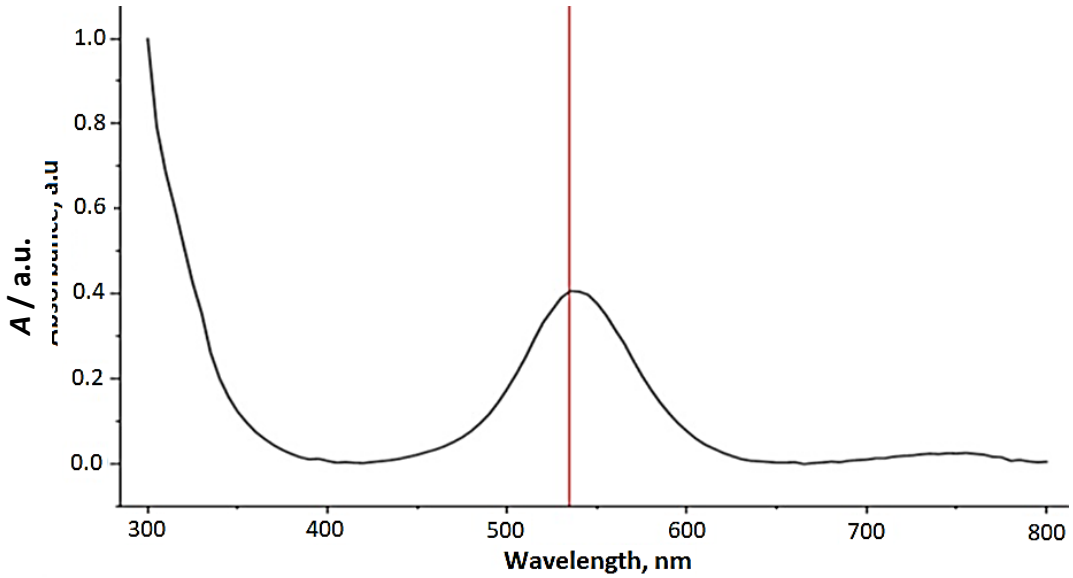

Figure 6*. UV-Vis spectrum of AuNPs sample F3 (optimal)*

In addition to particle size, a slight red-shift of the SPR peak can also be influenced by the refractive index of the surrounding medium. Bioactive molecules from the plum peel extract that cap the AuNPs surface may increase the local refractive index, leading to a shift of the SPR peak toward longer wavelengths. As discussed, *Prunus salicina* peel contains phenolic-rich constituents that can mediate metal-ion reduction due to their multiple aromatic rings and hydroxyl groups [11]. These polyphenolic

compounds can adsorb onto the gold surface during reduction, forming an organic capping layer that modifies the dielectric environment surrounding the nanoparticles. Such surface-bound biomolecules may therefore contribute to the observed LSPR position at 534.9 nm. The maximum absorbance value of 0.408 further indicates that a substantial concentration of nanoparticles was formed, sufficient to yield a clearly detectable optical response. Qualitatively, higher nanoparticle concentrations correspond to stronger (higher) LSPR peak intensities, as described by the Beer-Lambert law. Thus, the single peak at 534.9 nm confirms the successful synthesis of gold nanoparticles using plum peel extract, producing a stable AuNPs colloid characterized by the distinct UV-Vis spectrum of nanoplasmonic LSPR. The slight red shift relative to the ideal position of ~520 nm expected for ~10 to 15 nm monodisperse AuNPs may arise from the relatively broad size distribution (3.5 to 31 nm), surface phytochemical capping layer, and small interparticle plasmon coupling effects. The plasmonic behaviour and surface modification induced by phenolic capping are expected to influence electron-transfer characteristics at the electrode interface, thereby enhancing electrochemical sensing performance.

Fourier transform infrared spectroscopy

To examine the chemical interactions and confirm the role of phytochemicals, FTIR characterization was performed on the synthesized gold nanoparticles. The resulting spectrum is shown in Figure 7. The band near 3197 cm^{-1} corresponds to O-H stretching vibrations, which are typically associated with hydroxyl groups present in phenolic compounds and residual moisture. The feature around 1635 cm^{-1} may arise from aromatic C=C stretching and/or H-O-H bending vibrations from residual water. Since AuNPs are dispersed in water without any additional organic matrix, the contribution from moisture cannot be ignored in this region. The band near 665 to 666 cm^{-1} is most likely influenced by atmospheric CO_2 (bending mode), which may overlap with the vibrations of the fingerprint region; therefore, it is not considered a diagnostic band for phytochemical-Au interactions.

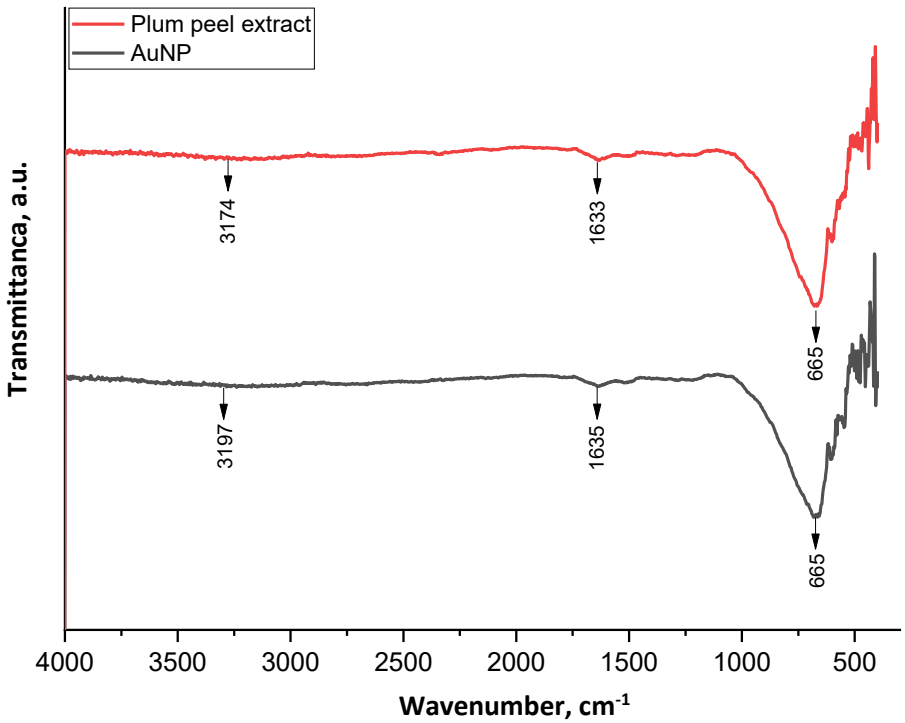

***Figure 7**. IR spectra of plum extract (red) and AuNPs (black)*

Comparison with the spectrum of the plum peel extract shows that several functional-group bands are retained after nanoparticle formation. Notably, the O-H stretching band shifts slightly from

~3174 cm^{-1} in the extract to ~3197 cm^{-1} in the AuNPs spectrum, indicating changes in the hydrogen-bonding environment and suggesting the involvement of hydroxyl-containing phytochemicals (*e.g.* polyphenols) in Au(III) reduction and/or nanoparticle stabilization. A minor shift is also observed in the ~1630 to 1640 cm^{-1} region (1633→1635 cm^{-1}), which may reflect subtle changes in aromatic/carbonyl-associated vibrations following nanoparticle formation [25,26]. The presence of aromatic-related bands in the AuNPs spectrum indicates that phytochemical constituents from the plum peel extract remain associated with the nanoparticle surface after reduction. These biomolecules likely act as both reducing agents and stabilizing (capping) agents.

During green synthesis, phenolic compounds can reduce Au(III) to Au(0) and subsequently adsorb onto the gold surface through interactions involving hydroxyl, carbonyl, and π-electron systems. Therefore, the observed aromatic vibrations in the AuNPs spectrum are attributed to surface-bound phytochemicals rather than free molecules in solution [27]. This interpretation is further supported by the negative zeta potential (-33.4 mV), indicating the presence of surface-bound, oxygen-containing phytochemicals that contribute to electrostatic stabilization. The presence of such phenolic-derived surface functionalities is expected to influence interfacial electron-transfer behaviour at the electrode surface, thereby enhancing electrochemical sensing performance.

Transmission electron microscopy analysis

TEM characterization was performed on the AuNPs dispersion obtained under optimal synthesis conditions immediately after the green synthesis process. The TEM results revealed that the synthesized AuNPs exhibited a predominantly spherical morphology, with particle sizes ranging from 3.53 nm to 31.06 nm and an average diameter of approximately 13.16 nm (Figure 8). The moderate average size (~13 nm) suggests that phenolic-rich phytochemicals in the plum peel extract likely regulate nucleation and growth, preventing excessive particle coalescence and promoting predominantly isotropic nanoparticle formation.

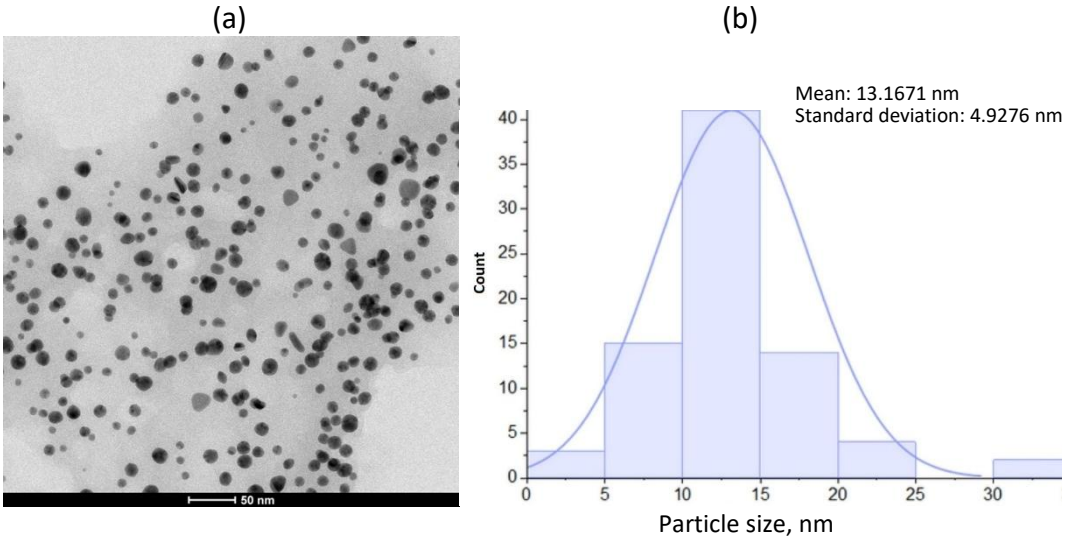

Figure 8. *(a) TEM micrograph and (b) particle size distribution of AuNPs synthesized in most optimal conditions*

The spherical morphology and nanoscale size distribution in the range of several tens of nanometres are consistent with numerous reports on the green synthesis of AuNPs using plant extracts or biopolymers. For instance, grape leaf (*Vitis vinifera*) extract has been reported to reduce Au(III) ions to form spherical AuNPs with sizes of approximately 10 to 17 nm [28]. Similarly, extract from *Amaranthus spinosus* produced gold nanoparticles with an average diameter of ~13 nm,

predominantly spherical in shape. These literature findings align well with the TEM observations in the present study, in which the green-synthesized AuNPs were uniformly distributed at the nanometre scale and exhibited a predominantly spherical morphology. As shown in Table 2, the average particle size obtained from plum peel extract (13.17 ± 4.9 nm) is comparable to the AuNPs synthesized using Tarap tree extract (12 to 25 nm, [26]). This similarity suggests that plant-based reducing agents, regardless of species differences, tend to promote the formation of small, spherical nanostructures due to the coordinated action of polyphenols and other bioactive compounds that regulate nucleation and growth. Although green synthesis methods may occasionally generate anisotropic shapes under certain phytochemical compositions or reaction conditions, the dominance of ~13 nm spherical AuNPs in this work indicates well-controlled reduction of Au(III) ions and stable, isotropic nanoparticle growth [29].

Table 2. *Comparison of AuNPs particle size synthesized by various plant extracts*

Plant extracts	Particle size, nm	Ref.
Tarap tree (*Artocarpus odoratissimus*)	12 to 25	[26]
Prunus cerasifera pissardii nigra leaf	103	[30]
Madhuca indica flower extract	20	[31]
Plum peels (*Prunus salicina)*	13.16 ± 4.9	This work

A characteristic feature of spherical AuNPs is the presence of an LSPR peak in the visible region. In this study, the UV-Vis spectrum exhibited an absorption maximum at $\lambda \approx 534.9$ nm (with an absorbance of ~0.408) for the synthesized AuNPs dispersion. The peak at approximately 535 nm indicates the surface plasmon band of gold and can be directly compared with values reported in the literature. Generally, small spherical AuNPs (~5 to 20 nm) display an LSPR peak around 520 nm, which progressively red-shifts as the particle size increases [32]. For instance, AuNPs with an average diameter of ~9 nm typically exhibit an LSPR maximum near 517 nm, while larger particles (~48 nm) show a red-shifted peak around 533 nm. Similar trends have been reported for green-synthesized AuNPs with spherical morphologies, where particles sized 15 to 35 nm show a surface plasmon resonance (SPR) band near 534 nm, while smaller particles (~5 to 10 nm) exhibit peaks between 520 and 526 nm. Therefore, the observed peak at ~534.9 nm in this study falls within the expected range for spherical AuNPs with diameters spanning the tens-of-nanometres scale. This slightly red-shifted value, compared to the ideal ~520 nm expected for pure 13 nm particles [33], may result from a broader size distribution (with some larger particles present) or mild particle aggregation, leading to plasmon coupling and red-shifted resonance. Overall, the UV-Vis (λ_{max} = 534.9 nm) and TEM (average diameter = 13 nm) results are consistent and complementary: both confirm the successful formation of spherical AuNPs, with the plasmonic shift remaining in good agreement with the measured particle size, albeit suggesting the presence of a minor fraction of larger particles.

Zeta potential

Zeta potential analysis was conducted to evaluate the electrostatic interactions between particles and, to assess the colloidal stability of the synthesized AuNPs. The optimized AuNPs exhibited a consistently high negative surface charge in three independent measurements, yielding ζ = -33.5, -33.2 mV and -33.4 mV, respectively (mean = -33.4 ± 0.2 mV). As widely reported in the literature, colloidal nanoparticles with $|\zeta| \geq 30$ mV are considered electrostatically stable due to sufficient repulsive forces that prevent aggregation. The measured $\zeta \approx$ -33 mV therefore places the synthesized AuNPs within the category of highly stable colloids, indicating strong electrostatic

stabilization conferred by the negatively charged phytochemical residues adsorbed on the nanoparticle surface. Plant-derived polyphenols, flavonoids, and organic acids commonly impart such negative charges, leading to a robust electrical double layer that effectively counteracts van der Waals attraction. This result stands in clear contrast to unstable colloids with zeta potentials near zero; unlike such systems, the present AuNPs dispersion does not undergo rapid sedimentation. Visual observations corroborate the zeta potential data: the AuNPs suspensions remained well dispersed for extended periods without noticeable settling, consistent with the thermodynamic stability expected at $|\zeta| > 30$ mV. Kalantari and Turner [34], for example, reported that nanoparticles require at least ±20 to ±30 mV to maintain sufficient repulsive energy to prevent aggregation, a criterion well exceeded by the present system.

The dispersion medium exhibited a conductivity of approximately 0.139 to 0.154 mS cm^{-1}, indicating a modest ionic environment adequate to sustain an electrical double layer without being so conductive as to compress it. This balance favours stable colloidal behaviour and supports the formation of well-dispersed, uniformly charged particles [35].

In the context of electrode modification, a stable and negatively charged AuNPs dispersion is advantageous, as it facilitates more homogeneous surface coverage during drop-casting onto the PGE. The presence of phenolic-derived surface functionalities and stable nanoparticle dispersion is expected to support efficient interfacial electron-transfer processes, thereby contributing to improved electrochemical sensing performance. For instance, it has already been demonstrated [36,37] that the incorporation of gold nanoparticles into carbon-based electrodes significantly improves voltammetric signal response by enhancing electron-transfer kinetics and increasing the effective electroactive surface area. A similar improvement is expected in the present work, supported by the high colloidal stability of the green-synthesized AuNPs. As shown in Table 3, the zeta potential of the plum peel-derived AuNPs (-33.4 ± 0.2 mV) is comparable to that reported for other plant-mediated syntheses, such as tarap tree extract (-35.74 mV).

Table 3. *Comparison of zeta potentials of various plant extracts*

Plant extracts	Zeta potential, mV	Ref.
Tarap tree (*Artocarpus odoratissimus*)	-35.74	[26]
Madhuca indica flower extract	~ 35	[31]
Prunus cerasifera pissardii nigra leaf	-27	[30]
Plum peels (*Prunus salicina*)	-33.4 ± 0.2	This work

Surface characterization of bare and gold nanoparticle-modified pencil graphite electrode

Scanning electron microscopy analysis

SEM operates by scanning the sample surface with a focused electron beam to generate high-resolution images of surface topography. SEM characterization is highly relevant for electrochemical sensors because the electrode surface morphology directly influences sensor performance. Surface modification with nanomaterials, such as AuNPs, typically increases the effective surface area and the number of active sites on the electrode.

As shown in Figure 9, at low magnification (50×), the surface of the unmodified PGE appears relatively smooth and homogeneous. In contrast, after modification with AuNPs (PGE/AuNPs), the surface becomes slightly rougher on the macroscopic scale. The morphological differences become more pronounced at higher magnification (2500×). The bare PGE image shows graphite structures arranged in flat, flake-like layers with large pores or gaps between them. Conversely, the PGE/AuNPs surface appears much rougher and more heterogeneous; the gold nanoparticle layer covers nearly

the entire electrode surface and fills the gaps between the graphite layers. The nanosized Au particles are observed as clusters distributed over the electrode surface, forming micro-clusters approximately 4 µm in size. These micro-clusters of aggregated AuNPs are distinctly different from the smoother morphology of the bare electrode, indicating successful deposition and surface modification.

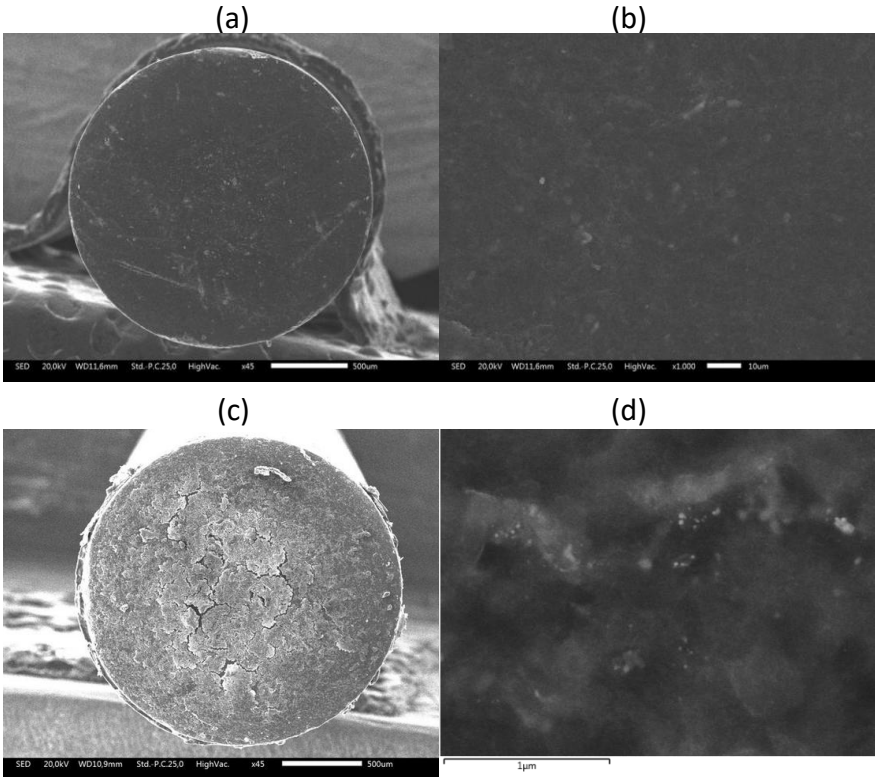

Figure 9. *SEM micrographs of: (a) bare PGE at 50× magnification, (b) bare PGE at 2500× magnification, (c) PGE/green-AuNPs at 50× magnification and (d) PGE/green-AuNPs at 2500× magnification*

The aggregation of AuNPs into larger clusters can be explained by the characteristics of the drop-casting process. As the solvent evaporates, the AuNPs are drawn toward the droplet edge and accumulate there due to the “coffee-ring” effect, resulting in a non-uniform distribution on the surface. Although the AuNPs were synthesized *via* a green route using plum peel extract rich in proanthocyanidins, where the proanthocyanidins act as both reducing agents for Au(III) to Au(0) and as capping ligands on the nanoparticle surface, the multi-layer drop-casting and extended drying time (approximately 8 hours per layer) led to particle coalescence and aggregation. This observation is consistent with reports in the literature, which state that drop-casting often produces large nanoparticle aggregates near the droplet edges due to the coffee-ring effect, in contrast to the smooth surface of bare PGE. These findings confirm that the modification successfully formed an AuNPs layer on the electrode, enhancing its roughness and increasing the electrochemically active surface area.

Energy dispersive X-ray spectroscopy analysis

In the SEM analysis, EDX was also performed to determine the elemental composition of the synthesized sample, as shown in Figure 10. The resulting EDX spectrum displayed dominant peaks corresponding to Au at characteristic energies around 2.1 and 9.7 keV, confirming the presence of metallic gold in the formed nanoparticles. The strong Au signal further indicates that the drop-casting method effectively anchored the gold nanoparticles onto the graphite electrode surface.

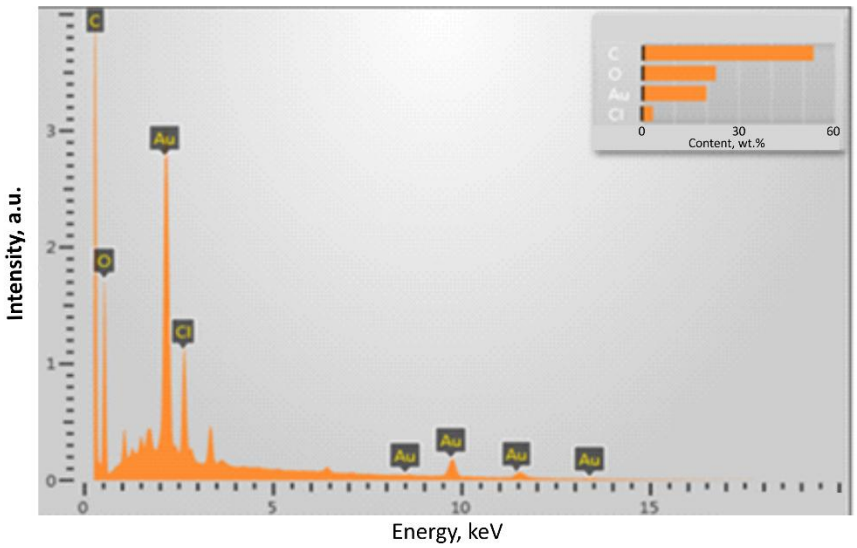

***Figure 10**. EDX spectrum of PGE/AuNPs*

The EDX elemental mapping confirms the successful deposition and spatial distribution of gold nanoparticles on the pencil graphite electrode surface (Figure 11). The carbon (C Kα) and oxygen (O Kα) maps show a relatively uniform background, characteristic of the graphite matrix and residual surface oxides. In contrast, the Au Mα map displays distinct, brightly concentrated regions corresponding to localized clusters of gold nanoparticles. When overlaid, the composite map reveals that Au is not randomly scattered but forms well-distributed domains across the electrode surface, indicating effective adherence of the green-synthesized AuNPs to the graphite substrate. This distribution pattern suggests that the drop-casting process yielded a consistent nanoparticle coating, which is expected to enhance the electroactive surface area and facilitate improved electron-transfer kinetics during voltammetric detection.

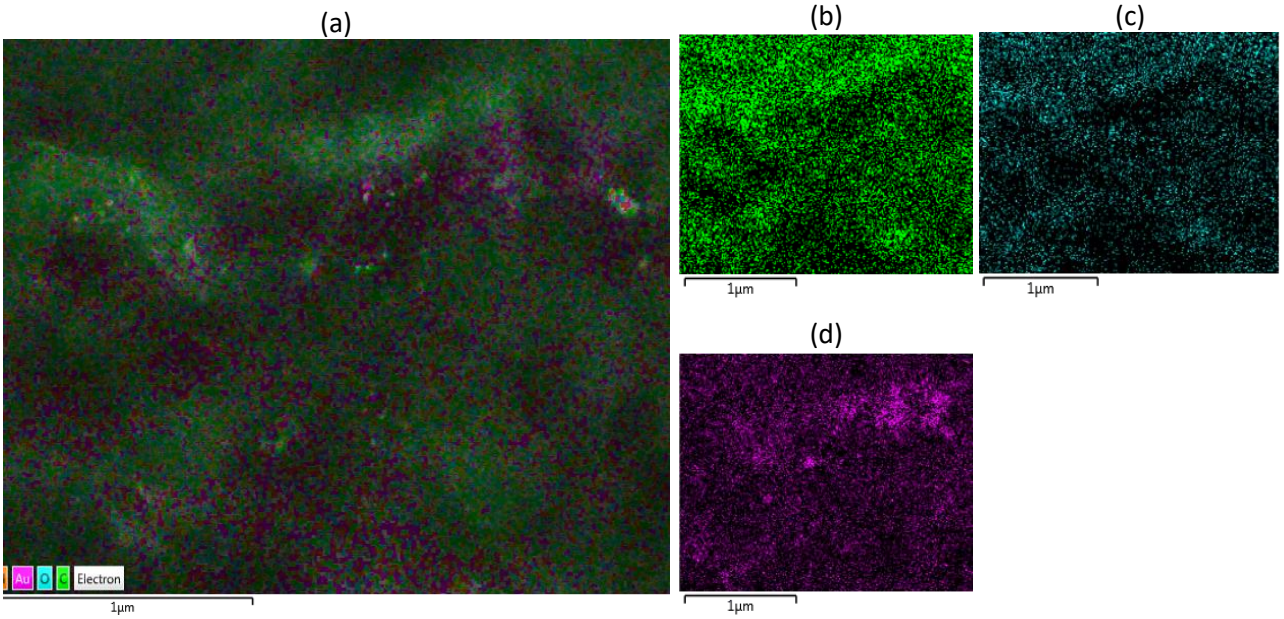

***Figure 11.** EDX elemental mapping of PGE/AuNPs: (a) overlay map showing the spatial distribution of elements; (b) carbon (green); (c) oxygen (blue); and (d) gold (purple)*

The EDX spectrum of the AuNPs-modified graphite electrode revealed four major elements, *i.e.*, carbon, oxygen, chlorine, and gold, with quantitative contributions of 53.36 wt.% C, 23.00 wt.% O, 3.52 wt.% Cl and 20.12 wt.% Au (Table 4).

Table 4. *EDX spectrum results for PGE/AuNPs*

Element	Line type	Apparent concentration, wt.%	*k* ratio	Content, wt.%	Content, at. %	Standard label
C	K series	35.11	0.35109	53.36 ± 0.41	73.04	C Vit
O	K series	23.56	0.07928	23.00 ± 0.34	23.64	SiO_2
Cl	K series	6.07	0.05306	3.52 ± 0.08	1.63	NaCl
Au	M series	35.03	0.35027	20.12 ± 0.31	1.68	Au

The dominant carbon signal originates from the graphite substrate, whereas the relatively high oxygen content reflects the presence of plant-derived organic molecules from the plum peel extract that remain adsorbed on the nanoparticle surfaces. These biomolecules, rich in polyphenols, flavonoids, and other oxygen-containing functional groups, serve as natural reducing and capping agents during the green synthesis process, and their incorporation onto the AuNPs surface is a well-established characteristic of phytochemical-mediated nanoparticle formation. The detection of chlorine at 3.52 wt.% is consistent with the use of $HAuCl_4$ as the gold precursor, where incomplete removal of chloride residues or partial incorporation during nucleation can lead to residual Cl signals. Notably, the presence of a strong Au peak (20.12 wt.%) confirms successful deposition of gold nanoparticles onto the graphite surface. Similar EDX patterns, strong Au accompanied by C and O from organic capping layers, and minor Cl residues, have been widely reported in green-synthesized AuNPs systems, such as those described by Hatipoğlu *et al*. [30], further validating the formation and stabilization of phytochemical-capped AuNPs in this study.

Electrochemical performance of PGE/AuNPs for Pb(II) detection

Comparison between bare and modified pencil graphite electrode

The measurement of Pb(II) concentration at 50 ppm using differential pulse voltammetry (DPV) revealed a distinct difference in response between the unmodified PGE and the AuNPs-modified PGE. DPV was selected as the detection technique due to its high sensitivity, excellent peak resolution, and low background (capacitive) current, achieved through the measurement of current differences before and after each potential pulse [38]. These advantages make DPV particularly suitable for detecting trace levels of heavy metals in aqueous solutions [39].

In this experiment, a 50 ppm Pb(II) standard solution was prepared, to which 0.1 M KCl was added as the supporting electrolyte. DPV measurements were conducted using an Ag/AgCl reference electrode, which provides a stable and constant reference potential. A platinum (Pt) wire was used as the counter electrode for its high conductivity and chemical inertness, thereby forming a conventional three-electrode electrochemical system [40].

As seen in Figure 12, in the DPV voltammogram of the 50 ppm Pb(II) solution, a clear oxidation peak of Pb(II) was observed at approximately -0.5 to -0.4 V *vs.* Ag/AgCl. The peak current was substantially higher with the AuNPs-modified PGE than with the bare PGE.

Quantitatively, the DPV peak current for Pb(II) at 50 ppm on the PGE/AuNPs electrode was recorded at approximately 42.59 µA, whereas the bare PGE produced a peak current of only about 28.25 µA. Therefore, surface modification of the electrode with AuNPs enhanced the Pb(II) detection current by 50.7 % compared to the unmodified graphite pencil electrode. This significant signal enhancement demonstrates the effectiveness of AuNPs in improving the electrochemical sensing performance.

The increase in the Pb(II) oxidation current observed for the AuNPs-modified electrode can be attributed to the presence of gold nanoparticles on the surface, which expands the electroactive surface area and enhances the electronic conductivity of the electrode [41].

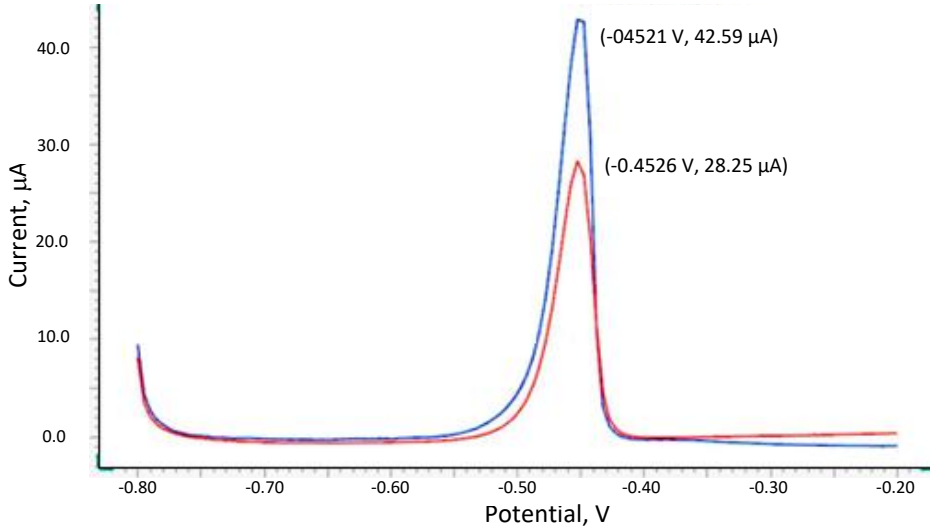

Figure 12. *DPVs of bare PGE (red) and PGE/AuNPs (black) recorded for the detection of 50 ppm Pb(II) in 0.5 M KCl. Measurement parameters: start potential -0.8 V, stop potential -0.2 V, step potential 5 mV, modulation amplitude 25 mV, and modulation time 0.05 s*

AuNPs provide a much larger surface area than bare graphite, allowing more Pb(II) ions to interact and adsorb onto the electrode surface. In addition, AuNPs serve as catalytic sites and provide more efficient electron-transfer pathways [42]. This observation is consistent with reports in the literature stating that electrode modification with gold nanoparticles increases the number of reactive sites and accelerates electron transfer, ultimately leading to higher sensitivity and current response. Furthermore, gold exhibits an underpotential deposition (UPD) phenomenon toward Pb(II), meaning that Pb(II) ions can be reduced to metallic Pb(0) on the gold surface at potentials more positive than those required for bulk deposition. This behaviour is evident from the slight positive shift in peak potential: the oxidation peak of Pb(II) on the bare PGE appeared at -0.4526 V, while on the PGE/AuNPs electrode it shifted to -0.4521 V [39]. In other words, even without a separate deposition step, Pb(II) ions could be spontaneously reduced to a Pb(0) monolayer on the AuNPs surface when polarized to negative potentials, and subsequently re-oxidized to Pb(II) during the DPV scan. These results are consistent with previous studies reporting that nanomaterial modifications, such as AuNPs on carbon-based electrodes, improve sensitivity and lower the detection limit for heavy metals compared to bare electrodes [43]. Therefore, the presence of AuNPs on the PGE surface significantly enhances sensor performance for Pb(II) detection, particularly at higher concentrations, yielding stronger, more distinguishable current signals and a slight positive shift in potential.

Analytical performance at trace levels

To further evaluate the sensor's performance at trace concentrations, the PGE/AuNPs electrode was used to measure Pb(II) solutions in the range of 25 to 200 ppb. The same reference, counter electrodes, and measurement parameters as described previously were employed. The resulting DPV voltammograms exhibited a regular increase in peak current with increasing Pb(II) concentration in the solution (Figure 13).

The voltammetric peak of Pb(II) in Figure 13 appeared consistently at approximately -0.4 V across all tested concentrations, while the peak current increased proportionally with concentration. A linear relationship between the peak current (I_p) and Pb(II) concentration was observed in the range of 25 to 200 ppb, indicating good sensor performance within this concentration range. This linear correlation is consistent with the quantitative nature of DPV, in which the peak height is directly proportional to the analyte concentration within a defined linear range.

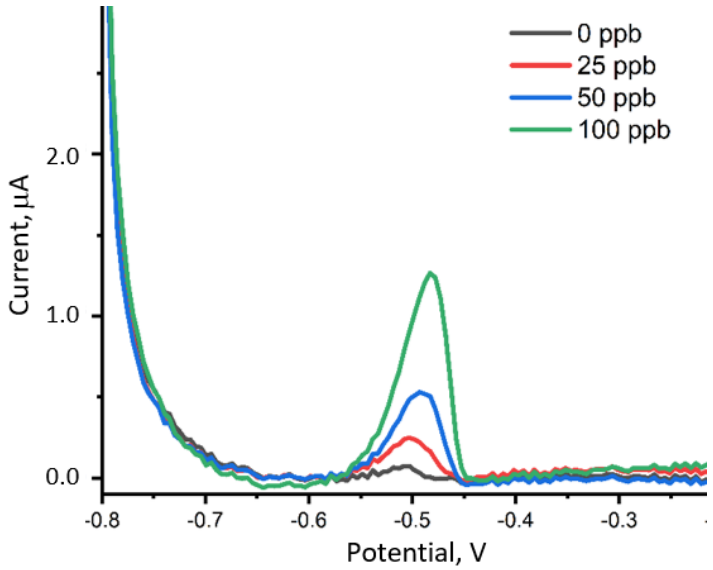

Figure 13. *DPVs of PGE/AuNPs in standard solutions of 25 to 100 ppb of Pb(II), measured in 0.5 M KCl, with start potential -0.8 V, stop potential -0.2 V, step 5 mV, modulation amplitude 25 mV and modulation time of 0.05 s*

A calibration curve with an excellent coefficient of determination (R^2 = 0.9921) was obtained, demonstrating highly linear behaviour across the concentration range of 25 to 200 ppb (Figure 14). This strong linearity ($R^2 > 0.99$) indicates that the electrochemical response of the PGE/AuNPs sensor is directly proportional to Pb(II) concentration within the tested range. From the regression equation $y = 0.0172x - 0.2964$, the slope of 17.2 nA ppb^{-1} represents the sensor sensitivity. This means that for every 1 ppb increase in Pb(II) concentration, the peak current increases by approximately 17.2 nA under the applied DPV conditions. Such sensitivity is consistent with the expected enhancement provided by the AuNPs modification, which increases the electroactive surface area and facilitates faster electron-transfer kinetics.

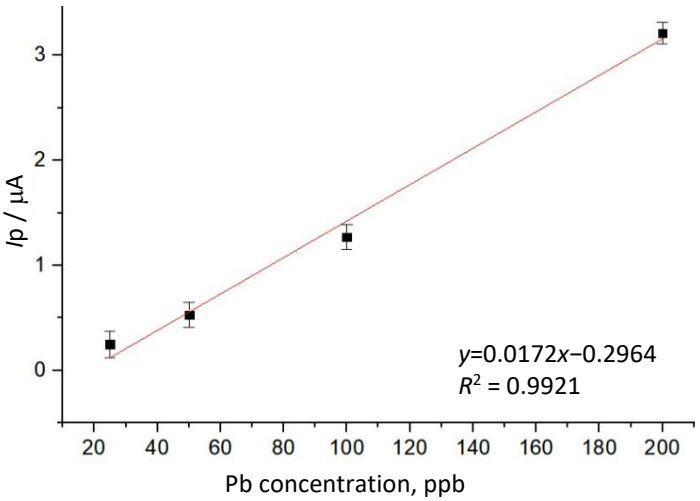

Figure 14. *Calibration curve of PGE/AuNPs for low concentrations of Pb(II) solutions obtained by DPV with start potential -0.8 V, stop potential -0.2 V, step 5 mV, modulation amplitude 25 mV and modulation time of 0.05 s*

At the lowest tested concentration (25 ppb), the sensor produced a clearly distinguishable peak current of approximately 0.2 to 0.3 µA, demonstrating that the electrode can reliably detect Pb(II) at trace levels with a high signal-to-noise ratio. The linear trend across all four calibration points further confirms the stability and reproducibility of the modified electrode. This performance aligns well with previous reports showing that pencil graphite electrodes (PGEs), especially when modified with metal nanoparticles, exhibit superior analytical performance in pulse voltammetric techniques

such as DPV, owing to their low background noise and favourable electron-transfer characteristics. Overall, the PGE/AuNPs-based sensor demonstrates excellent analytical capability for trace Pb(II) detection, highlighting its potential for rapid and reliable on-site monitoring applications.

Furthermore, the sensor performance was evaluated in terms of the limit of detection (LOD) and limit of quantification (LOQ). The LOD is defined as the lowest concentration that can be detected with statistical significance, whereas the LOQ represents the lowest concentration that can be quantified with acceptable precision. In this study, both LOD and LOQ were calculated based on the standard deviation (σ) of the signal at the lowest detectable concentration and the slope (S) of the calibration curve [44].

Standard deviation of the blank signal was estimated from the standard deviation of the peak currents obtained at 25 ppb of Pb(II), which was the lowest detectable concentration. The limit of detection and limit of quantification for the PGE/AuNPs sensor were determined to be 18.95 and 63.17 ppb, respectively. This means that, theoretically, the sensor can detect Pb(II) ions at concentrations as low as approximately 19 ppb, while accurate quantification is possible above 63 ppb. The obtained LOD in the tens of Pb(II) range is considered satisfactory, especially given that no anodic stripping or pre-deposition step was employed during the measurement.

For comparison, Wan *et al*. [42] reported a carbon dot/AuNPs-based SPCE sensor for heavy metal detection using DPV (without mercury plating), achieving a Pb(II) LOD of about 4.2 ppb [42]. Although this value is lower than that obtained in the present study, the modification

used in their system was more complex, involving two types of nanomaterials. In contrast, the PGE/AuNPs sensor developed in this work successfully detected Pb(II) at concentrations below 20 ppb through a simpler fabrication approach. The slightly higher LOD observed here could be further improved in future work by optimizing the nanoparticle synthesis or incorporating a low-potential deposition (open-circuit preconcentration) step prior to the DPV scan.

When comparing sensors produced *via* green synthesis routes (Table 5), the PGE modified with plum peel-derived AuNPs (LOD = 18.95 ppb) exhibits a clear performance advantage over the CPE/green RGO sensor prepared from cork tree peel (LOD = 62.2 ppb). This represents roughly a threefold improvement in detection capability, highlighting the superior electrochemical enhancement provided by gold nanoparticles relative to RGO. The smaller particle size, higher conductivity, and greater density of active sites on the AuNPs-modified surface collectively contribute to its lower detection limit, demonstrating the effectiveness of plum peel-based AuNPs as a sustainable and highly sensitive sensing material. Nevertheless, when compared with the study conducted by Elobeid *et al.* [45], who employed an unmodified pencil graphite electrode (PGE) for the detection of lead in groundwater using differential pulse voltammetry (DPV) with anodic stripping, the reported LOD was 45 µM (9.32 ppm). This finding demonstrates that modification with gold nanoparticles (AuNPs) can significantly enhance the analytical performance of PGE in Pb(II) detection. The linearity and sensitivity achieved in this study (range: 25 to 200 ppb; sensitivity: 17.2 nA ppb^{-1} represent an important step forward in the development of pencil graphite - based electrochemical sensors.

***Table 5**. Limit detection for lead (II) of various sensor types*

Type of sensor	LOD	Ref.
CPE/green RGO (from cork tree peel)	62.2 ppb	[46]
Carbon dot/AuNPs-based SPCE	4.2 ppb	[42]
PGE	9.32 ppm	[45]
PGE/green AuNPs (plum peels extracts)	18.95 ppb	This work

These results confirm that AuNPs-modified PGE has strong potential as a low-cost, effective electrochemical sensor for trace Pb(II) detection, offering a portable alternative to conventional instruments such as AAS or ICP-MS [47].

In other words, the present results confirm that gold nanoparticle modification markedly improves the voltammetric performance of PGE-based sensors, as evidenced by enhanced peak current, strong linearity in the ppb range, and a detection limit of 18.95 ppb. This LOD is lower than the maximum Pb(II) limit of 30 ppb stipulated for Class I-III surface waters under the Indonesian water-quality regulation (PP 82/2001), and far below the 1000 ppb limit for Class IV waters. Accordingly, the developed sensor is fit for purpose for environmental monitoring and early detection of Pb(II) contamination in surface waters, as it can detect concentrations below the relevant regulatory thresholds. However, for drinking-water applications, both the World Health Organization (WHO) and Indonesian health regulations specify a far stricter limit of 10 ppb for Pb(II). Since the current LOD of 18.95 ppb is still above this requirement, the sensor is not yet suitable for confirming compliance with drinking-water standards, although it remains highly effective for broader environmental surveillance. Overall, these findings underscore the strong potential of green-synthesized AuNPs for portable heavy-metal sensing and highlight clear pathways for future sensitivity enhancement.

Conclusions

This study successfully established an optimized and fully green route for synthesizing gold nanoparticles (AuNPs) using plum peel extract, yielding highly stable, uniformly capped, and predominantly spherical nanoparticles. The optimal precursor-to-extract ratio (7:3, 80 mL maceration solvent) produced a well-defined SPR peak at 534.9 nm, while FTIR, TEM, and zeta potential measurements (-33.4 ± 0.2 mV) confirmed effective phytochemical reduction, strong colloidal stability, and nanoscale particle uniformity.

When applied to pencil graphite electrodes (PGE), these green-synthesized AuNPs substantially enhanced electrochemical performance. The modified electrode delivered a 50.7 % increase in Pb(II) oxidation peak current, excellent linearity across trace concentrations (R^2 = 0.9921), a sensitivity of 0.0172 μA ppb^{-1}, and a limit of detection of 18.95 ppb. This detection limit is well below the regulatory threshold for class I to class III surface waters (30 ppb, PP 82/2001) [48], demonstrating that the sensor is not only analytically reliable but also fit for purpose for rapid environmental screening, while approaching, though not yet meeting, the stricter WHO drinking-water guideline of 10 ppb.

SEM-EDX mapping revealed homogeneous AuNPs coverage and confirmed the presence of catalytically active gold clusters that facilitate faster electron transfer, validating the mechanistic basis for the observed analytical improvement. Overall, the PGE/AuNPs platform presented here is low-cost, disposable, easy to fabricate, and compatible with a portable potentiostat, making it a strong candidate for field-deployable, in-situ monitoring of Pb(II) contamination. The valorisation of fruit peel waste further enhances the sustainability and scalability of this approach, underscoring its promise for next-generation green electrochemical sensors.

Conflict of Interest: *The authors declare no conflict of interest.*

Acknowledgements*: The authors would like to acknowledge E-Layanan Sains, National Research and Innovation Agency (BRIN), for providing laboratory instrument facilities. The authors also acknowledge the effective collaboration between the Study Center of Sensor and Green Chemistry, Faculty of Mathematics and Natural Sciences, Universitas Padjadjaran and the Research Center for Electronics, Research Organization for Electronics and Informatics, BRIN*

Funding: *This research received no external funding.*

Use of artificial intelligence*: The authors used AI-assisted tools only for language editing and clarity improvement. All scientific content and conclusions are the responsibility of the authors.*

References

[1] E. Supriyantini, N. Soenardjo, Kandungan Logam Berat Timbal (Pb) Dan Tembaga (Cu) Pada Akar Dan Buah Mangrove Avicennia marina Di Perairan Tanjung Emas Semarang, *Jurnal Kelautan Tropis* **18** (2016) 98-106. https://doi.org/10.14710/JKT.V18I2.520 (In Indonesian)

[2] G. Lantu, V. S. Kamu, H. F. Aritonang, Sintesis Nanokomposit Nata de Coco/Grafena Oksida Sebagai Adsorben Ion Logam Timbal, *Chemistry Progress* **17** (2024) 60-67. https://doi.org/10.35799/CP.17.1.2024.54310 (In Indonesian)

[3] M. Dicky, N. Putra, S. Widada, W. Atmodjo, Studi Kandungan Logam Berat Timbal (Pb) pada Sedimen Dasar di Perairan Banjir Kanal Timur Semarang, *Indonesian Journal Oceanography* **4** (2022) 13-21. https://doi.org/10.14710/IJOCE.V4I3.13398 (In Indonesian)

[4] H. Dogruyol, İ. C. Tunçelli, Ö. Özden, N. Erkan, F. S. Karakulak, Bioaccumulation of Mercury, Cadmium, Lead, and Arsenic in Whiting and Tub Gurnard From the Sea of Marmara: Implications for Human Health, *Food Science & Nutrition* **13** (2025) e70370. https://doi.org/10.1002/fsn3.70370

[5] M. Karundeng, Y. W. Hartati, Parameter analisis voltammetri pulsa diferensial elektrode grafit pensil untuk penentuan kadmium, *Fullerene Journal of Chemistry* **2** (2017) 82-91. https://doi.org/10.37033/FJC.V2I2.15 (In Indonesian)

[6] B. Pavan Venkatachala, S. Manjappa, B. E. Kumara Swamy, L. S. Manjunatha, Pre-treated pencil graphite modified electrode sensor for melatonin, *Journal of Electrochemistry Science and Engineering* **15** (2025) 2594. https://doi.org/10.5599/jese.2594

[7] S. N. Zakiyyah, N. P. Satriana, N. Fransisca, S. Gaffar, N. Syakir, Irkham, Y. W. Hartati, Gold nanoparticle-modified screen-printed carbon electrodes for label-free detection of SARS-CoV-2 RNA using drop casting and spray coating methods, *ADMET and DMPK* **13** (2025) 2577. https://doi.org/10.5599/admet.2577

[8] N. Sarfraz, I. Khan, Plasmonic Gold Nanoparticles (AuNPs): Properties, Synthesis and their Advanced Energy, Environmental and Biomedical Applications, *Chemistry - An Asian Journal* **16** (2021) 720-742. https://doi.org/10.1002/ASIA.202001202

[9] W. Li, Z. Cao, R. Liu, L. Liu, H. Li, X. Li, Y. Chen, C. Lu, Y. Liu, AuNPs as an important inorganic nanoparticle applied in drug carrier systems, *Artificial Cells, Nanomedicine, and Biotechnology* **47** (2019) 4222-4233. https://doi.org/10.1080/21691401.2019.1687501

[10] S. Casalinuovo, D. Caschera, S. Quaranta, D. Caputo, AuNP-Decorated Textile as Chemo Resistive Sensor for Acetone Detection, *IEEE Sensors Journal* **25** (2025) 7757-7762. https://doi.org/10.1109/JSEN.2023.3348693

[11] M. Jawad, M. Ali, S. Qasim, A. Akbar, N. A. Khan, M. B. Sadiq, Determination of Phenolic Compounds and Bioactive Potential of Plum (Prunus salicina) Peel Extract Obtained by Ultrasound-Assisted Extraction, *BioMed Research International* **2022** (2022) 7787958. https://doi.org/10.1155/2022/7787958

[12] M. Gallo, A. Formato, M. Ciaravolo, G. Formato, D. Naviglio, Study of the Kinetics of Extraction Process for The Production of Hemp Inflorescences Extracts by Means of Conventional Maceration (CM) and Rapid Solid-Liquid Dynamic Extraction (RSLDE), *Separations* **7** (2020) 20. https://doi.org/10.3390/SEPARATIONS7020020

[13] L. Shi, W. Zhao, Z. Yang, V. Subbiah, H. A. R. Suleria, Extraction and characterization of phenolic compounds and their potential antioxidant activities, *Environmental Science and Pollution Research* **29** (2022) 81112-81129. https://doi.org/10.1007/S11356-022-23337-6

[14] A. Mokrani, K. Madani, Effect of solvent, time and temperature on the extraction of phenolic

compounds and antioxidant capacity of peach (*Prunus persica L.*) fruit, *Separation and Purification Technology* **162** (2016) 68-76. https://doi.org/10.1016/J.SEPPUR.2016.01.043
[15] V. Vorobyova, M. Skiba, K. Vinnichuk, G. Vasyliev, Synthesis of gold nanoparticles using plum waste extract with green solvents, *Sustainable Chemistry for the Environment* **6** (2024) 100086. https://doi.org/10.1016/J.SCENV.2024.100086
[16] H. Tyagi, A. Kushwaha, A. Kumar, M. Aslam, A Facile pH Controlled Citrate-Based Reduction Method for Gold Nanoparticle Synthesis at Room Temperature, *Nanoscale Research Letters* **11** (2016) 362. https://doi.org/10.1186/S11671-016-1576-5
[17] M. H. Fakhr, N. Beshchasna, S. Balakin, I. L. Carrasco, A. Heitbrink, F. Göhler, N. Rösch, J. Opitz, Cleaning of LTCC, PEN, and PCB Au electrodes towards reliable electrochemical measurements, *Scientific Reports* **12** (2022) 20431. https://doi.org/10.1038/s41598-022-23395-3
[18] A. P. Lima, G. L. Nunes, R. G. Franco, R. Mariano-Neto, G. S. Oliveira, E. M. Richter, E. Nossol, R. A. A. Munoz, Al_2O_3 microparticles immobilized on glassy-carbon electrode as catalytic sites for the electrochemical oxidation and high detectability of naproxen: Experimental and simulation insights, *Journal of Electroanalytical Chemistry* **882** (2021) 114988. https://doi.org/10.1016/J.JELECHEM.2021.114988
[19] S. Srinivas, A. Senthil Kumar, Surface-Activated Pencil Graphite Electrode for Dopamine Sensor Applications: A Critical Review, *Biosensors* **13** (2023) 353. https://doi.org/10.3390/BIOS13030353
[20] S. Farooq, F. Wali, D. M. Zezell, R. E. de Araujo, D. Rativa, Optimizing and Quantifying Gold Nanospheres Based on LSPR Label-Free Biosensor for Dengue Diagnosis, *Polymers* **14** (2022) 1592. https://doi.org/10.3390/POLYM14081592
[21] P. K. Ngumbi, S. W. Mugo, J. M. Ngaruiya, Determination of Gold Nanoparticles Sizes via Surface Plasmon Resonance, *IOSR Journal of Applied Chemistry (IOSR-JAC)* **11** (2018) 25-29. https://doi.org/10.9790/5736-1107012529
[22] X. Zhang, M. Li, Y. Lv, X. Sun, Y. Han, B. Liu, X. Zhao, X. Huang, Probing gold nanoparticles for the desensitization to β-lactoglobulin from binding mechanism, structure and IgE binding changes, *Food Chemistry* **342** (2021) 128329. https://doi.org/10.1016/J.FOODCHEM.2020.128329
[23] Z. Ashikbayeva, A. Bekmurzayeva, Z. Myrkhiyeva, N. Assylbekova, T.S. Atabaev, D. Tosi, Green-synthesized gold nanoparticle-based optical fiber ball resonator biosensor for cancer biomarker detection, *Optics & Laser Technology* **161** (2023) 109136. https://doi.org/10.1016/J.OPTLASTEC.2023.109136
[24] T. A. Sathya, S. Viswanathan, A. Basha, G. Jahirhussain, S. Alagumanian, S. Sobana, N. Arumugam, Environmental profiling of gold nanoparticles by flavonoids fractionalization from *carrica papaya* leaf extract for photocatalytic debasement of organic contaminants and it's cyto-toxic analysis, *Environmental Research* **259** (2024) 119445. https://doi.org/10.1016/j.envres.2024.119445
[25] H. Veisi, M. Farokhi, M. Hamelian, S. Hemmati, Green synthesis of Au nanoparticles using an aqueous extract of Stachys lavandulifolia and their catalytic performance for alkyne/aldehyde/amine A^3 coupling reactions, *RSC Advances* **8** (2018) 38186-38195. https://doi.org/10.1039/c8ra06819d
[26] M. Isa, S. Aid, R. Ali, Y. Asako, K. Shameli, A. Jonny, H. Zazuli, M. Taib, M. Yusefi, Green synthesis of gold nanoparticles via *Artocarpus odoratissimus* peel extract for potential applications of optical filter and catalytic degradation, *Journal of King Saud University - Science* **36** (2024) 103209. https://doi.org/10.1016/j.jksus.2024.103209
[27] N. Roy, B. Ghosh, D. Roy, B. Bhaumik, M. N. Roy, Exploring the Inclusion Complex of a Drug (Umbelliferone) with α-Cyclodextrin Optimized by Molecular Docking and Increasing

Bioavailability with Minimizing the Doses in Human Body, *ACS Omega* **5** (2020) 30243-30251. https://doi.org/10.1021/ACSOMEGA.0C04716

[28] J. Santhoshkumar, S. Rajeshkumar, S. Venkat Kumar, Phyto-assisted synthesis, characterization and applications of gold nanoparticles - A review, *Biochemistry and Biophysics Reports* **11** (2017) 46-57. https://doi.org/10.1016/J.BBREP.2017.06.004

[29] S. Link, M. A. El-Sayed, Size and Temperature Dependence of the Plasmon Absorption of Colloidal Gold Nanoparticles, *The Journal of Physical Chemistry B* **103** (1999) 4212-4217. https://doi.org/10.1021/JP984796O

[30] A. Hatipoglu, Green synthesis of gold nanoparticles from Prunus cerasifera pissardii nigra leaf and their antimicrobial activities on some food pathogens, *Progress in Nutrition* **23(3)** (2021) e2021241. https://doi.org/10.23751/pn.v23i3.11947

[31] D. Saha, D. Talukdar, P. Mukherjee, D. Mitra, R. Mukherjee, S. Guha, A. Bhattacharjee, R. Naskar, K. Sahu, N. Alam, G. Das, N. Murmu, Green synthesis of gold nano-particles using *Madhuca indica* flower extract and their anticancer activity on head and neck cancer : Characterization and mechanistic study, *European Journal of Pharmaceutics and Biopharmaceutics* **207** (2025) 114625. https://doi.org/10.1016/j.ejpb.2025.114625

[32] N. Dalal, B. S. Boruah, A. Neoh, R. Biswas, Correlation of Surface Plasmon Resonance Wavelength (SPR) with Size and Concentration of Noble Metal Nanoparticles, *Annals Reviews & Research* **5** (2019) 555658. https://doi.org/10.19080/ARR.2019.05.555658

[33] M. A. Dheyab, J. H. Tang, A. A. Aziz, S. H. Nowfal, M. S. Jameel, M. Alrosan, N. Oladzadabbasabadi, M. Ghasemlou, Green synthesis of gold nanoparticles and their emerging applications in cancer imaging and therapy: a review, *Reviews in Inorganic Chemistry* **45** (2024) 663-685. https://doi.org/10.1515/revic-2024-0048

[34] H. Kalantari, R. J. Turner, Structural and antimicrobial properties of synthesized gold nanoparticles using biological and chemical approaches, *Frontiers in Chemistry* **12** (2024) 1482102. https://doi.org/10.3389/fchem.2024.1482102

[35] M. I. Skiba, I. L. Kovalenko, Y. M. Skyba, V. I. Vorobyova, Capping Agent-Free Aqueous Gold Nanoparticles Generated By an Environmentally Friendly Plasma-Liquid Method, *Voprosy Khimii i Khimicheskoi Tekhnologii* (2024) 121-130. https://doi.org/10.32434/0321-4095-2024-156-5-121-130

[36] N. Kusnin, N. A. Yusof, N. A. A. Mutalib, F. Mohammad, J. Abdullah, S. Sabri, S. Mustafa, A. F. M. Saman, F. N. M. Faudzi, A. A. Soleiman, Enhanced Electrochemical Conductivity of Surface-Coated Gold Nanoparticles/Copper Nanowires onto Screen-Printed Gold Electrode, *Coatings* **12** (2022) 622. https://doi.org/10.3390/coatings12050622

[37] S. Kolahi-Ahari, B. Deiminiat, G. H. Rounaghi, Modification of a pencil graphite electrode with multiwalled carbon nanotubes capped gold nanoparticles for electrochemical determination of tramadol, *Journal of Electroanalytical Chemistry* **862** (2020) 113996. https://doi.org/10.1016/J.JELECHEM.2020.113996

[38] Y. T. Yaman, S. Abaci, Sensitive Adsorptive Voltammetric Method for Determination of Bisphenol A by Gold Nanoparticle/Polyvinylpyrrolidone-Modified Pencil Graphite Electrode, *Sensors* **16** (2016) 756. https://doi.org/10.3390/S16060756

[39] S.A . Tukur, N .A. Yusof, R. Hajian, Gold Nanoparticles-Modified Screen-Printed Electrode for Determination of Pb(II) Ion Using Linear Sweep Anodic Stripping Voltammetry, *IEEE Sensors Journal* **15** (2015) 2780-2784. https://doi.org/10.1109/JSEN.2014.2379283

[40] R. Mamińska, A. Dybko, W. Wróblewski, All-solid-state miniaturised planar reference electrodes based on ionic liquids, *Sensors and Actuators B* **115** (2006) 552-557. https://doi.org/10.1016/j.snb.2005.10.018

[41] M. Chelly, S. Chelly, R. Zribi, H. Bouaziz-ketata, R. Gdoura, N. Lavanya, G. Veerapandi, C. Sekar, G. Neri, Synthesis of Silver and Gold Nanoparticles from *Rumex roseus* Plant Extract and Their

Application in Electrochemical Sensors, *Nanomaterials* **11** (2021) 739. https://doi.org/10.3390/NANO11030739

[42] H. Wan, Q. Sun, H. Li, F. Sun, N. Hu, P. Wang, Screen-printed gold electrode with gold nanoparticles modification for simultaneous electrochemical determination of lead and copper, *Sensors and Actuators B* **209** (2015) 336-342. https://doi.org/10.1016/J.SNB.2014.11.127

[43] G. Martínez-Paredes, M. B. González-García, A. Costa-García, In situ electrochemical generation of gold nanostructured screen-printed carbon electrodes. Application to the detection of lead underpotential deposition, *Electrochimica Acta* **54** (2009) 4801-4808. https://doi.org/10.1016/J.ELECTACTA.2009.03.085

[44] V. Barwick, M. Bravo, R. Ellison, J. Egman, F. Gjengedal, O. Lund, *Eurachem Guide: The Fitness for Purpose of Analytical Methods - A Laboratory Guide to Method Validation and Related Topics*, Eurachem, 2014, p. 31-35 https://www.eurachem.org/images/stories/Guides/pdf/MV_guide_3rd_ed_V1_EN.pdf

[45] W. H. Elobeid, A. A. Elbashir, A. Ahmed Elbashir, Development and Validation of Differential Pulse Anodic Stripping Voltammetric Method for Determination of Lead (II) in Ground Water Using a Pencil Graphite Electrode, *EC Chemistry* **3(1)** (2018). https://ecronicon.net/assets/ecch/pdf/ECCH-03-00023.pdf

[46] I. B. Silva, D. Medeiros, D. Ara, M. Vocciante, S. Ferro, C. A. Mart, E. V. Dos Santos, Electrochemical Determination of Lead Using A Composite Sensor Obtained from Low-Cost Green Materials : Graphite / Cork, *Applied Sciences* **11** (2021) 2355. https://doi.org/10.3390/app11052355

[47] W. Ghann, T. Harris, D. Kabir, H. Kang, M. Jiru, M. M. Rahman, M. M. Ali, J. Uddin, Lipoic Acid Decorated Gold Nanoparticles and Their Application in the Detection of Lead Ions, *Journal of Nanomedicine & Nanotechnology* **10(5)** (2019) 539. https://doi.org/10.35248/2157-7439.19.10.539

[48] E. Indrawati, Z. Musada, A. G. Tantu, R. Renal, Status Pencemaran Logam Berat Timbal dan Kadmium di Sungai Tallo Menggunakan Bioindikator Ikan Nila *Oreochromis Niloticus*, *Jurnal Ilmiah Ecosystem* **22** (2022) 348-361. https://doi.org/10.35965/eco.v22i2.1562 (In Indonesian)